Science Advances
AAAS

Supplementary Materials for

Metallo-alginate hydrogel can potentiate microwave tumor ablation for synergistic cancer treatment

Yujie Zhu *et al.*

Corresponding author: Zhuang Liu, zliu@suda.edu.cn; Liangzhu Feng, lzfeng@suda.edu.cn

Sci. Adv. 8, eabo52885 (2022)
DOI: 10.1126/sciadv.abo5285

This PDF file includes:

Figs. S1 to S26

Fig. S1.

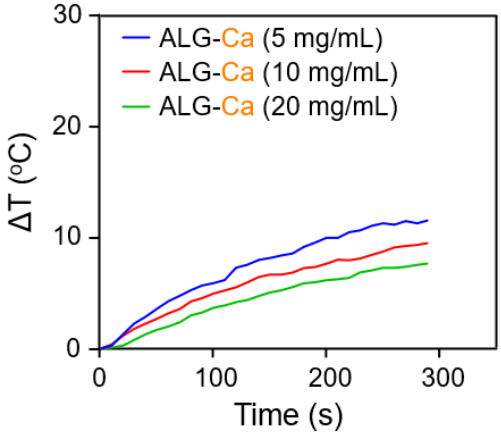

Figure S1. Microwave heating profiles of ALG-Ca hydrogels with a fixed Ca^{2+} concentration (50 mM) and different ALG concentrations as indicated.

Fig. S2.

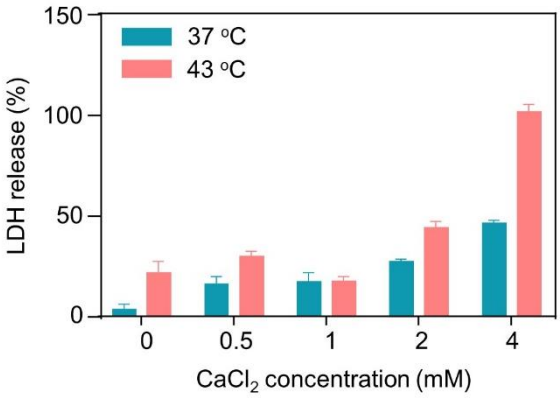

Figure S2. LDH release profile of CT26 cells incubated with different concentrations of $CaCl_2$ under 37 and 43 °C.

Fig. S3.

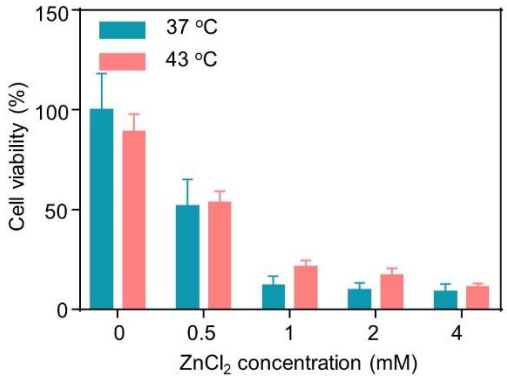

Figure S3. Relative cell viabilities of CT26 cells incubated with different concentrations of $ZnCl_2$ under 37 and 43 °C.

Fig. S4.

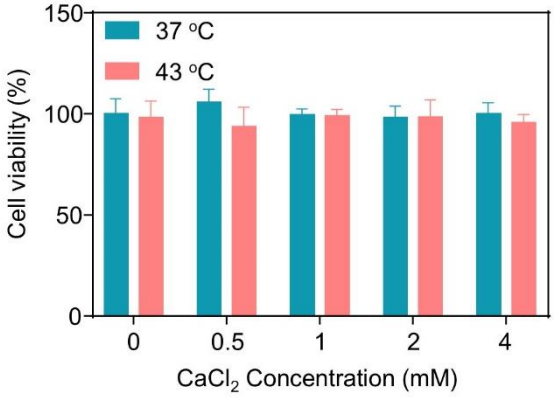

Figure S4. Relative cell viabilities of HUVEC cells incubated with different concentrations of $CaCl_2$ under 37 and 43 °C.

Fig. S5.

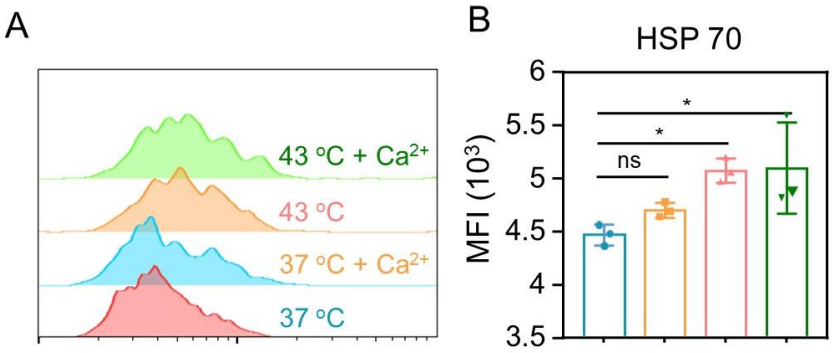

Figure S5. Flow cytometric analysis (A) and corresponding quantification of the mean fluorescence intensity (MFI, B) of intracellular HSP70 levels inside CT26 cells post various treatments as indicated by the color codes.

Fig. S6.

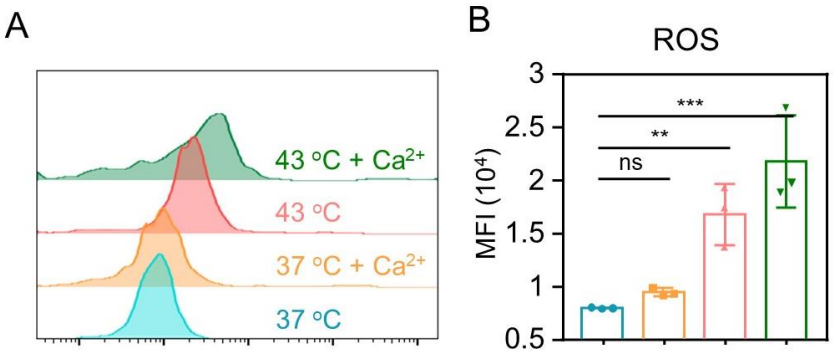

Figure S6. Flow cytometric analysis (A) and corresponding quantification of the mean fluorescence intensity (MFI, B) of ROS levels inside CT26 cells post various treatments as indicated by the color codes.

Fig. S7.

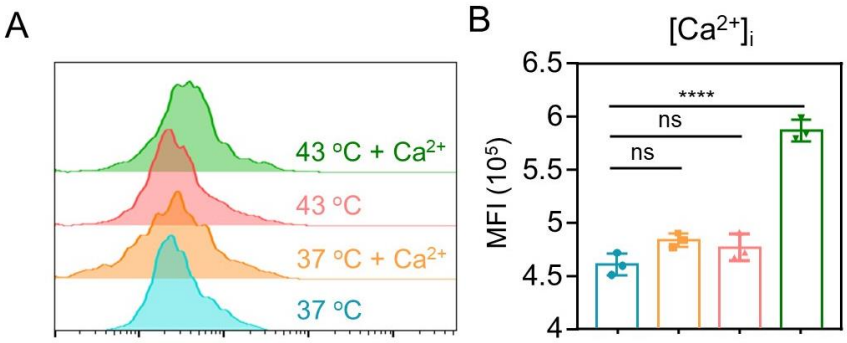

Figure S7. Flow cytometric analysis (A) and corresponding quantification of the mean fluorescence intensity (MFI, B) of intracellular Ca^{2+} levels inside CT26 cells post various treatments as indicated by the color codes.

Fig. S8.

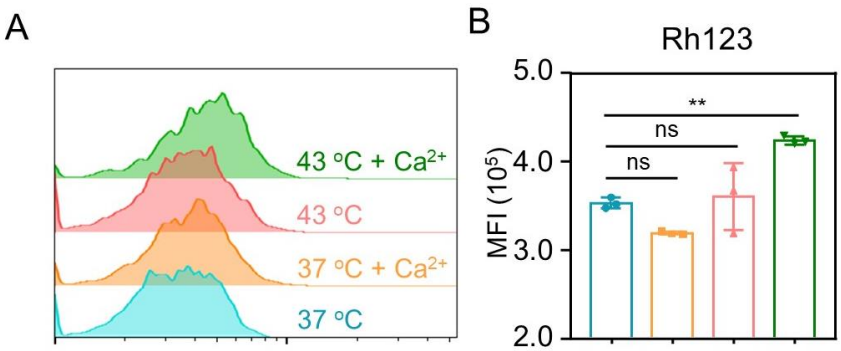

Figure S8. Flow cytometric analysis (A) and corresponding quantification of the mean fluorescence intensity (MFI, B) of mitochondrial membrane potential inside CT26 cells post various treatments as indicated by the color codes.

Fig. S9.

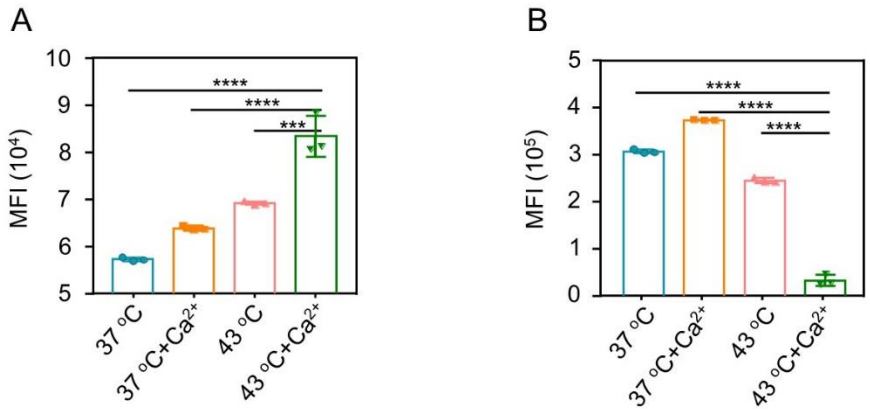

Figure S9. Semiquantitative analysis of (A) CRT expression and (B) HMGB1 release of CT26 cells post various treatments as indicated by recording their MFI based on the corresponding flow cytometric analysis.

Fig. S10.

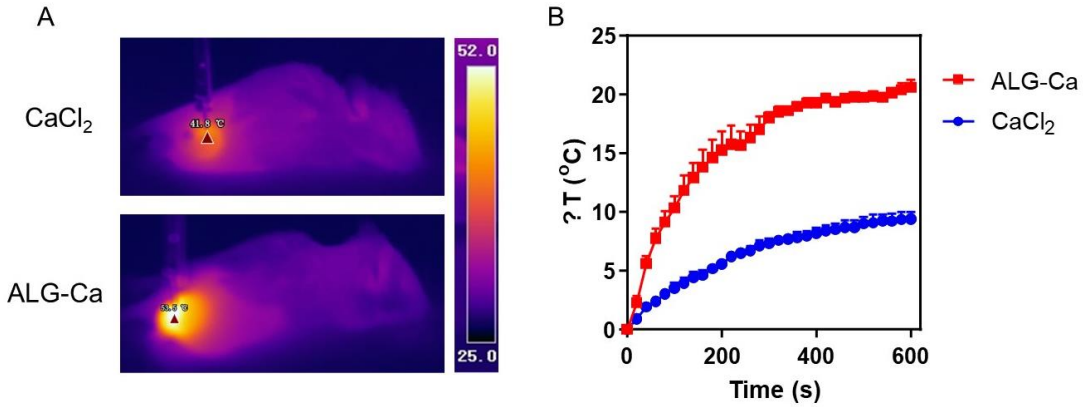

Figure S10. Thermal images (A) and heating profile (B) of $CaCl_2$ and ALG-Ca hydrogel in vivo.

Fig. S11.

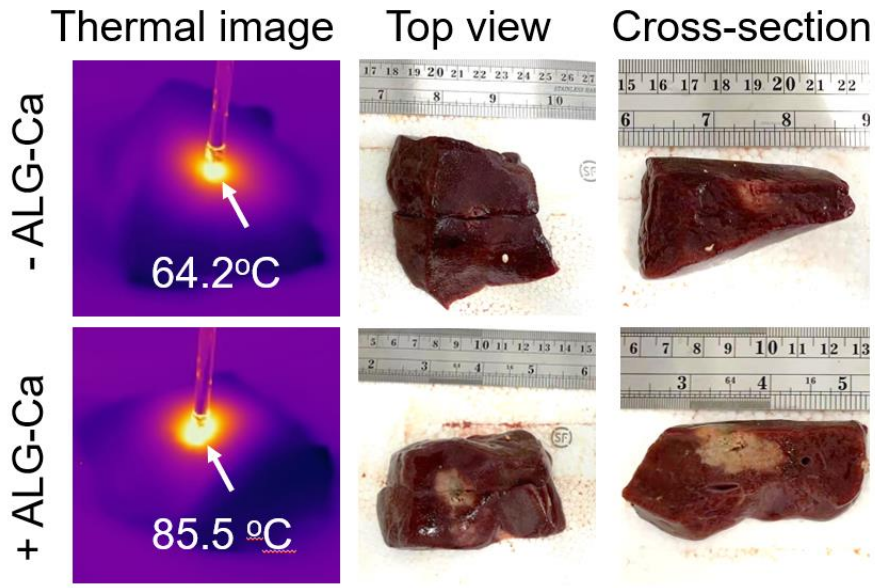

Figure S11. The thermal images and corresponding photographs of porcine liver with and without injections of Ca^{2+}-surplus ALG hydrogels (2 mL) under the microwave irradiation (15 W, 10 min).

Fig. S12.

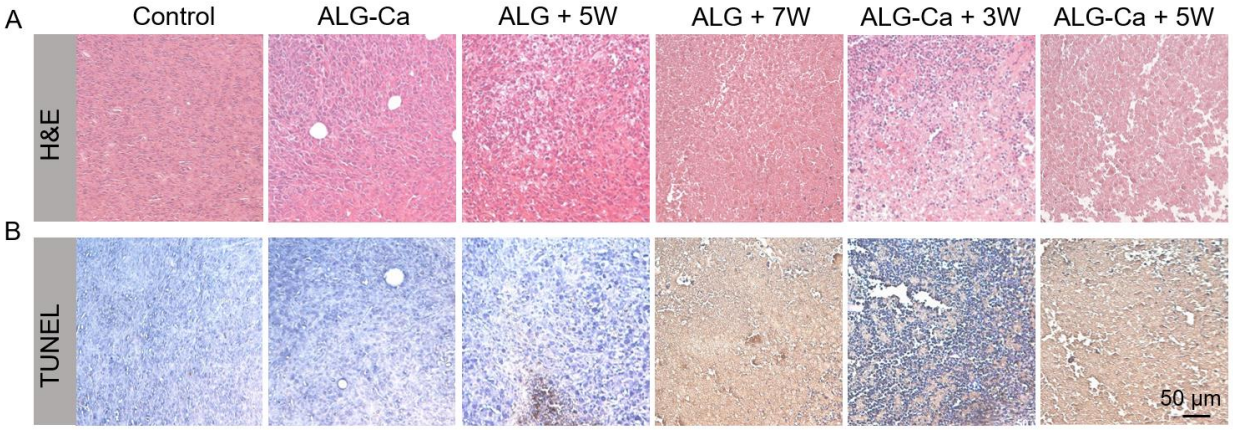

Figure S12. Evaluation of early-stage therapeutic efficacy of different treatments as indicated by the H&E (A) and TUNEL (B) staining.

Fig. S13.

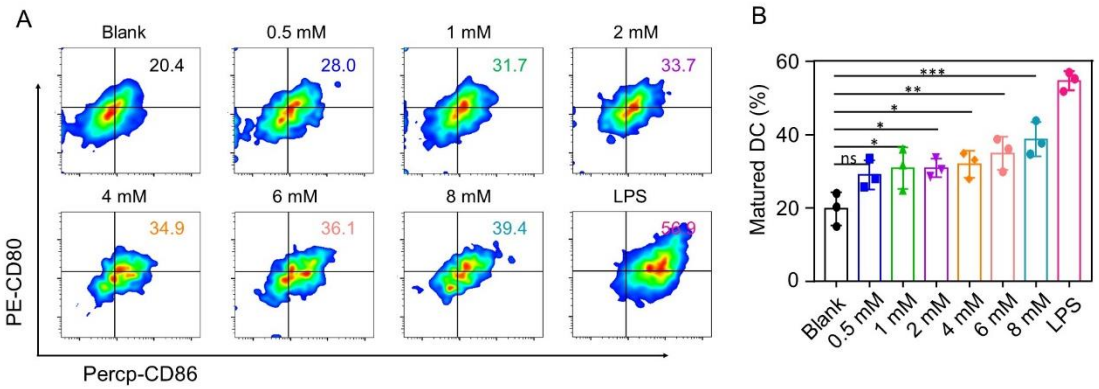

Figure S13. Flow cytometric analysis (A) and corresponding quantification (B) of maturity rate of BMDC cells incubated with different concentrations of $CaCl_2$.

Fig. S14.

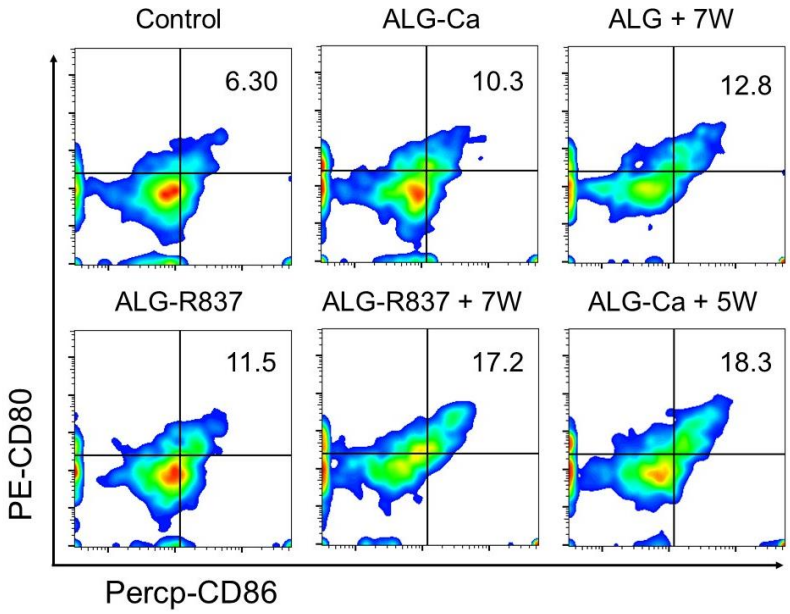

Figure S14. Representative flow cytometric analysis of the DC maturation in the drain lymph nodes adjacent to the primary tumors.

Fig. S15.

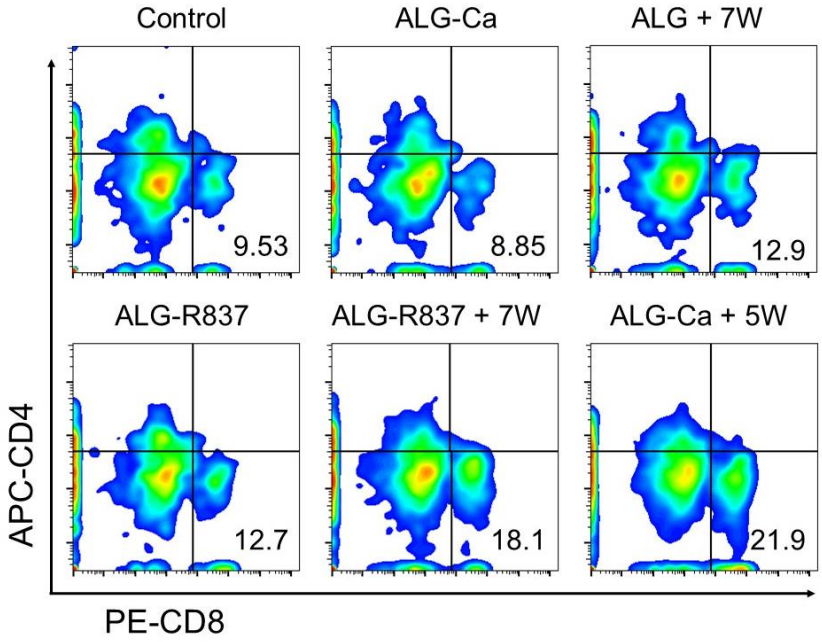

Figure S15. Representative flow cytometric analysis of $CD3^{+}CD8^{+}$ T cells inside the distant tumors post various treatments as indicated.

Fig. S16.

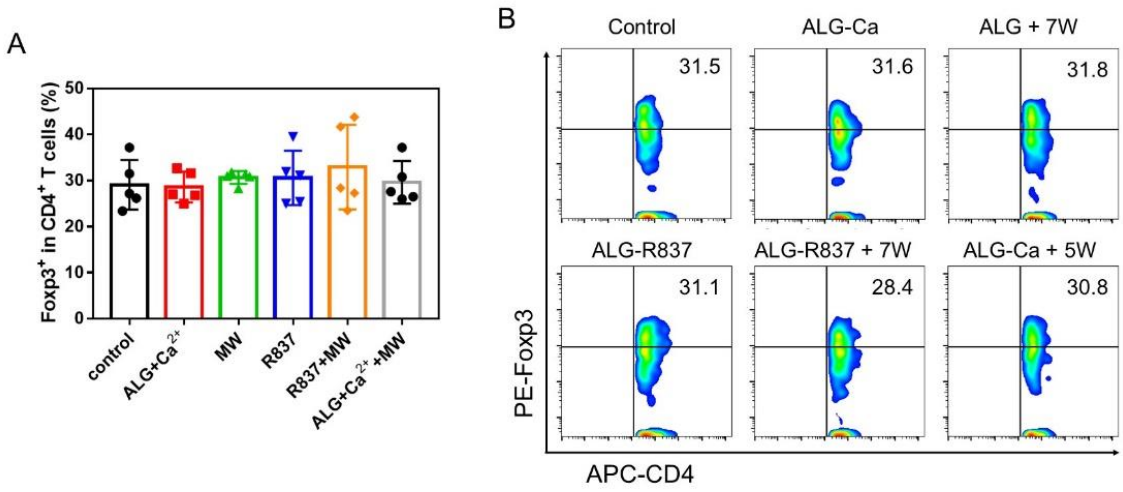

Figure S16. The statistical diagram (A) and representative flow cytometric diagram (B) of frequencies of $CD3^{+}CD4^{+}FoxP3^{+}$ Tregs inside the distant tumors post various treatments as indicated.

Fig. S17.

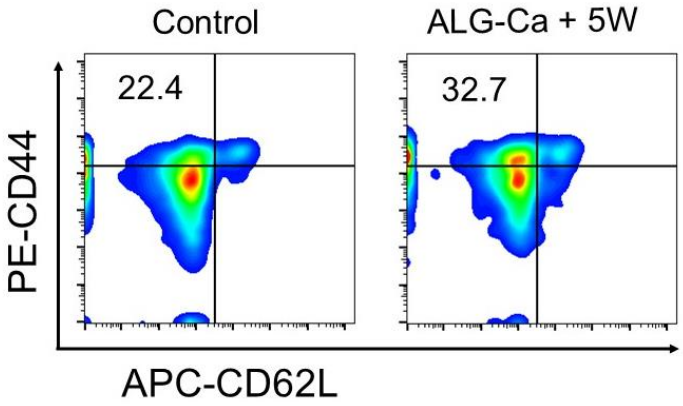

Figure S17. Representative flow cytometric analysis of $CD3^{+}CD8^{+}CD44^{+}CD62L^{-}$ T_{EM} cells in the peripheral blood collected from mice post various treatments as indicated.

Fig. S18.

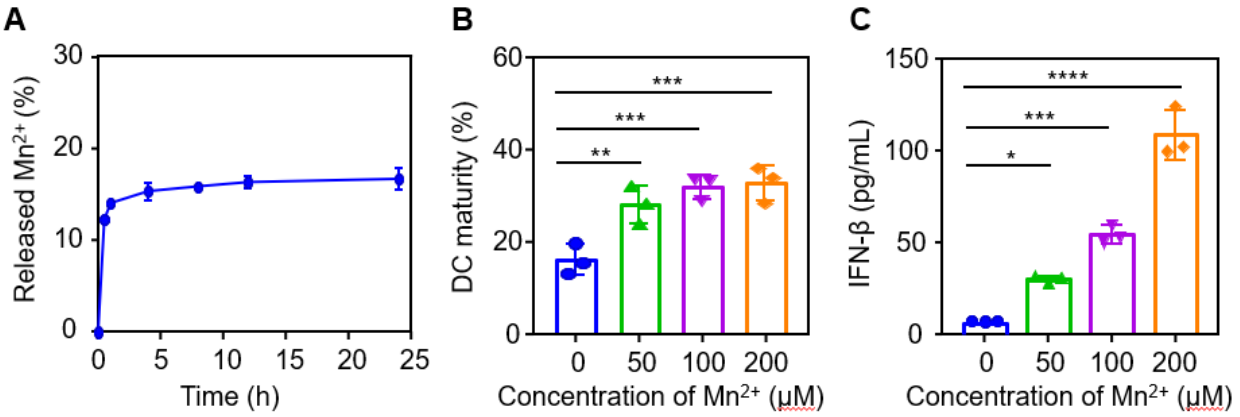

Figure S18. Characterization of ALG-Ca-Mn hydrogel. (A) Mn^{2+} release profile of ALG-Ca-Mn hydrogel. (B) Flow cytometric analysis of maturity rate of BMDC cells incubated with different concentration of $MnCl_2$. (C) IFN-β secretion levels of BMDC cells with different concentration of $MnCl_2$.

Fig. S19.

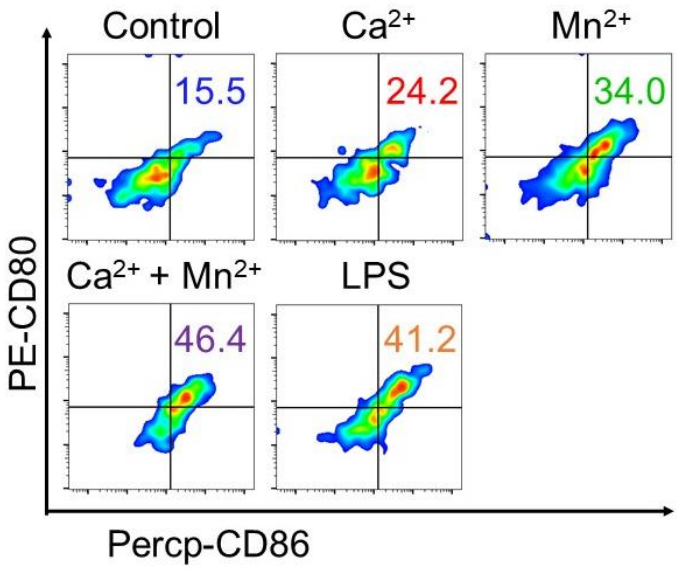

Figure S19. Flow cytometric analysis of maturity rates of BMDC cells received different treatments as indicated.

Fig. S20.

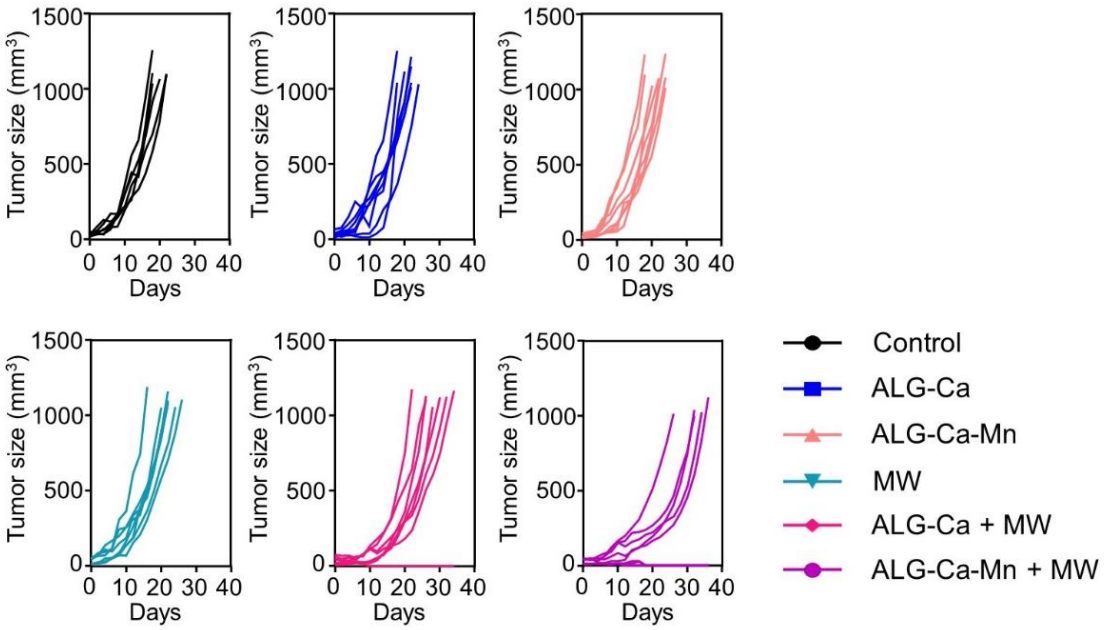

Figure S20. Individual tumor growth curves of distant tumors in mice post different treatments as indicated.

Fig. S21.

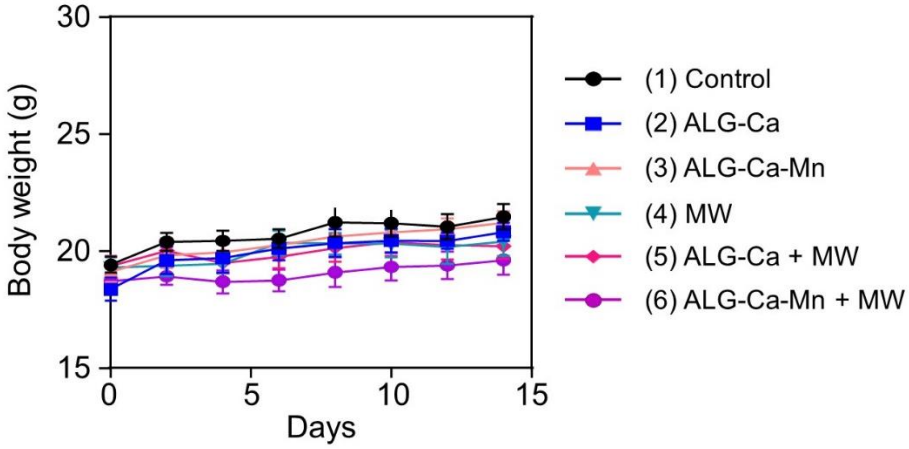

Figure S21. Body weights of mice post different treatments as indicated.

Fig. S22.

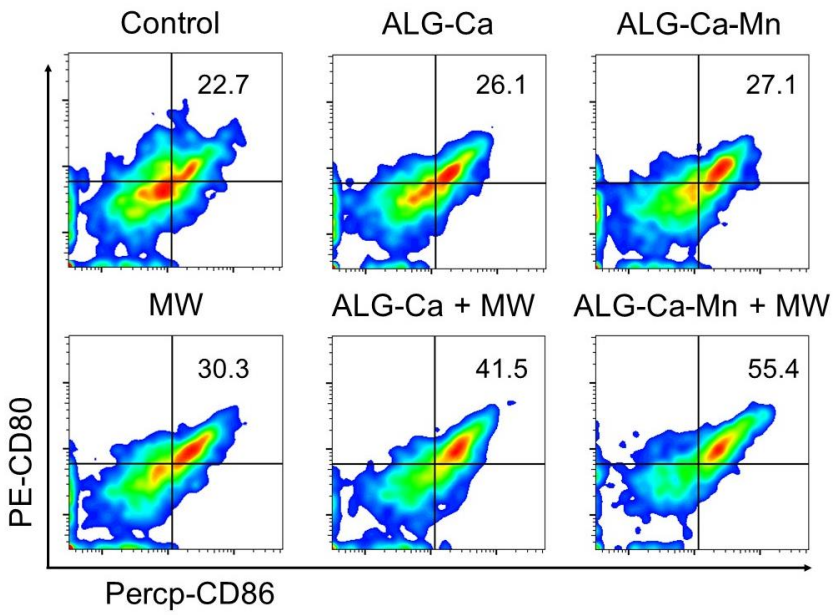

Figure S22. Representative flow cytometric analysis of the DC maturation in the drain lymph nodes adjacent to the primary tumors in mice with different treatments as indicated.

Fig. S23.

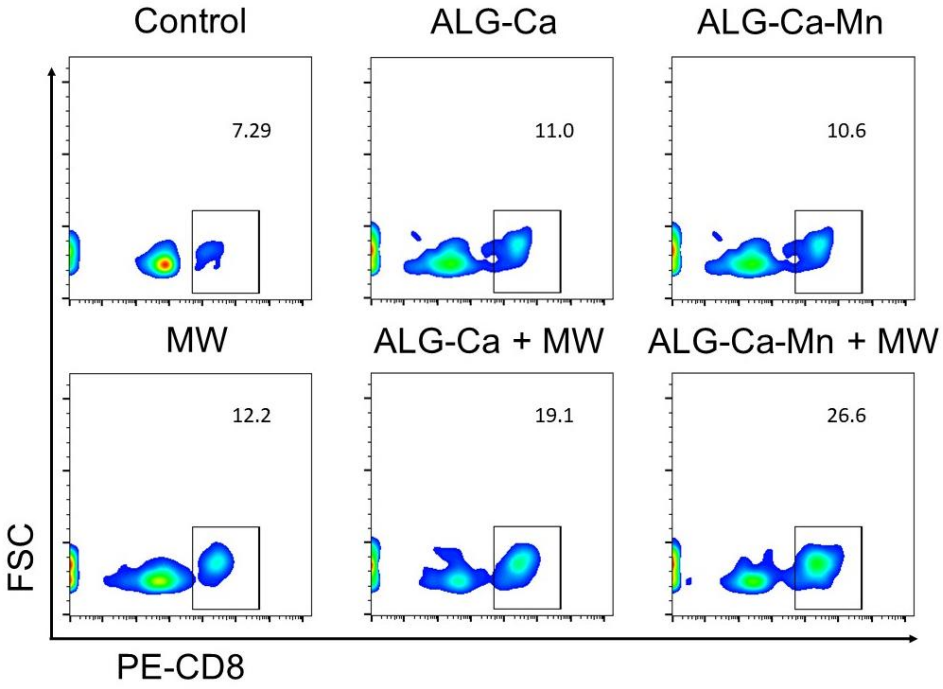

Figure S23. Representative flow cytometric analysis of $CD3^{+}CD8^{+}$ T cells inside the distant tumors in mice post various treatments as indicated.

Fig. S24.

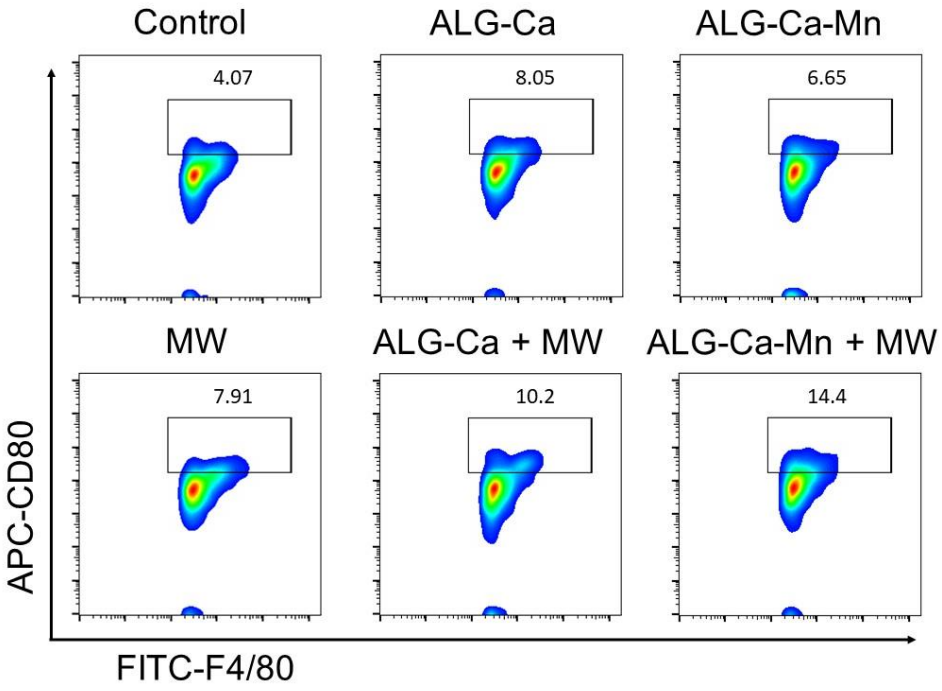

Figure S24. Representative flow cytometric analysis of $CD11b^{+}F4/80^{+}CD80^{+}$ M1 cells inside the distant tumors of mice post various treatments as indicated.

Fig. S25.

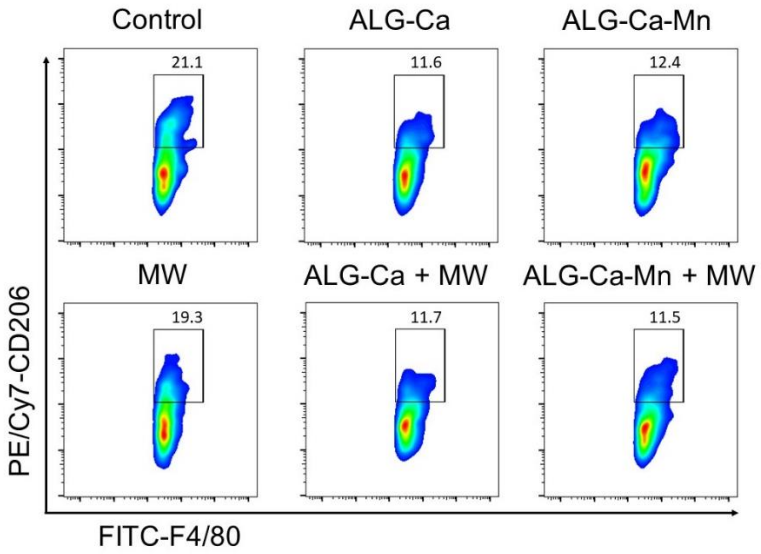

Figure S25. Representative flow cytometric analysis of $CD11b^{+}F4/80^{+}CD206^{+}$ M2 cells inside the distant tumors of mice post various treatments as indicated.

Fig. S26.

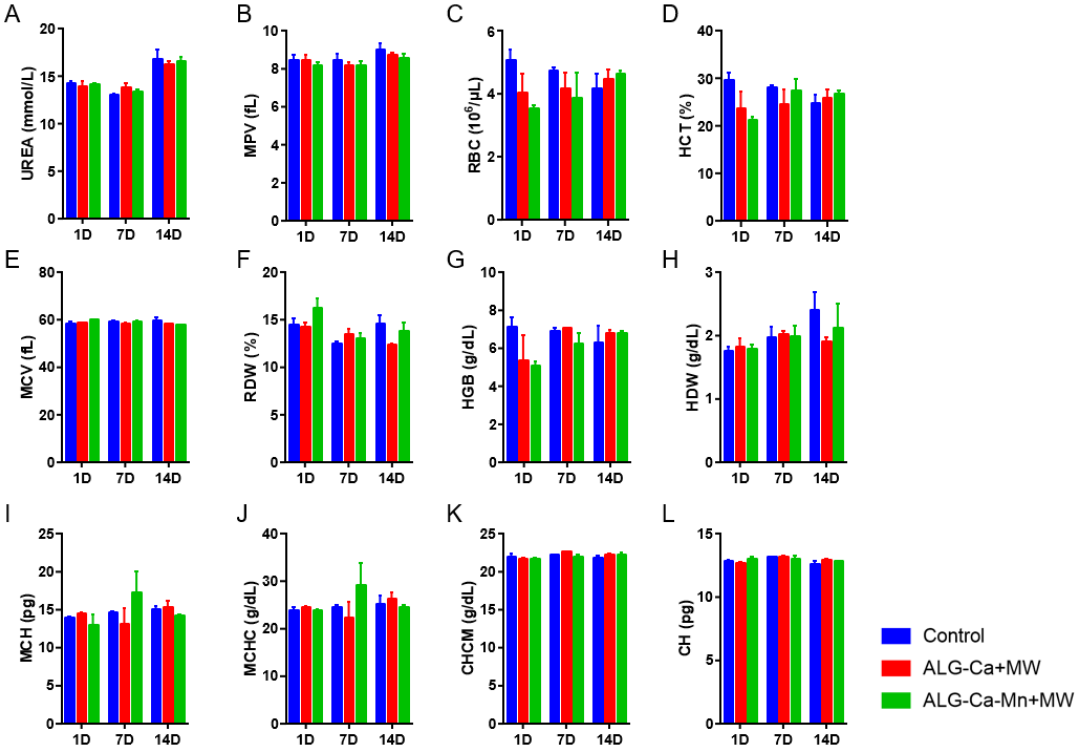

Figure S26. Blood biochemistry analysis and complete blood panel analysis of mice treated with PBS, ALG-Ca+MW and ALG-Ca-Mn+MW. (A) urea, (B) mean platelet volume (MPV), (C) red blood cells (RBC), (D) hematocrit (HCT), (E) mean corpuscular volume (MCV), (F) red blood cell distribution width (RDW), (G) hemoglobin (HGB), (H) hemoglobin distribution width (HDW), (I) mean corpuscular hemoglobin (MCH), (J) mean corpuscular hemoglobin concentration (MCHC), (K) cellular hemoglobin concentration mean (CHCM), (L) corpuscular hemoglobin (CH).